Volume 9, Issue 5, 2019, 4292 - 4300 ISSN 2069-5837

Biointerface Research in Applied Chemistry

www.BiointerfaceResearch.com

https://doi.org/10.33263/BRIAC95.292300

Original Research Article Open Access Journal

Received: 11.07.2019 / Revised: 05.09.2019 / Accepted: 10.09.2019 / Published on-line: 15.09.2019

Evaluation of the physicochemical, thermal and behavioural properties of consciousness energy healing treated iron (II) sulphate

Mahendra Kumar Trivedi [1], Snehasis Jana [2,*]

[1]Trivedi Global, Inc., Henderson, USA

[2]Trivedi Science Research Laboratory Pvt. Ltd., Thane (W), India

*corresponding author e-mail address: ***publication@trivedieffect.com***

ABSTRACT

Iron (II) sulphate is used as a source of iron to treat iron deficiency anemia. In this study evaluated the impact of the Trivedi Effect®-Consciousness Energy Healing Treatment on the physicochemical, thermal, and behavioural properties of iron sulphate using modern analytical techniques. Iron sulphate sample was divided into control and treated parts. Only treated sample received the Trivedi Effect®-Consciousness Energy Healing Treatment remotely by a famous Biofield Energy Healer, Mr. Mahendra Kumar Trivedi. The powder XRD relative peak intensities and crystallite size of the treated iron sulphate were significantly altered ranging from -87.25% to 338.67% and from -58.33% to 99.84%, respectively compared to the control sample. The average crystallite size of the treated iron sulphate was significantly decreased by 5.68% compared with the control sample. The particle size values of the treated iron sulphate was decreased by 1.54% (d_{10}), 1.12% (d_{50}), 2.51% (d_{90}), and 1.90% {D(4,3)} and the surface area was increased by 4.69% compared with the control sample. The melting temperature of the four peaks (1^{st}-4^{th}) of the treated sample was decreased by 0.28%, 12.45%, 5.44%, and 0.51%, respectively compared to the control sample. The latent heat of fusion of 1^{st}, 2^{nd}, and 4^{th} peaks in the treated sample was decreased by 47.29%, 75.39%, and 0.29%, respectively, whereas 3^{rd} peak was increased by 8.02% compared with the control sample. The total weight loss in the treated iron sulphate was increased by 0.78% compared with the control sample. The maximum thermal melting temperature of the treated sample was slightly increased by 2.03% in the 1^{st} peak; but decreased by 1.53%, 12.64%, and 1.27% in the 2^{nd}, 3^{rd}, and 4^{th} peaks, respectively compared to the control sample. Overall results suggested that the Trivedi Effect®-Consciousness Energy Healing Treatment might lead to the production of a new polymorphic form of iron sulphate, which would be more soluble and bioavailable, compared to the untreated sample. The Trivedi Effect® treated iron sulphate would be useful to design more efficacious nutraceutical/pharmaceuticals, which might offer better therapeutic response against iron deficiency anemia.

Keywords: *Iron sulphate, Energy of Consciousness Healing Treatment, The Trivedi Effect®, Crystallite size, Particle size, melting point, latent heat, weight loss.*

1. INTRODUCTION

Iron (II) sulphate (ferrous sulphate) has the molecular formula $FeSO_4 \cdot nH_2O$ and exist most commonly as heptahydrate (n = 7) form [1]. Traditionally it is known as "green vitriol" or "copperas", forms beautiful blue-green crystals of the monoclinic system. It is useful in chemistry as a reducing agent and as the best source of iron. The hydrated form of iron sulphate is used as medicine to treat iron deficiency anemia [2]. It was used in the manufacture of inks (iron gall ink) [3]. It is used for treating iron chlorosis in horticulture [4], lawn conditioner, moss killer, gold refining, purification of water, wood panelling on houses [5] and act as a catalyst (Fenton's reagent) in chemical reactions [6, 7].

Side effects associated with the internal use of iron sulphate are constipation, stomach upset, black or dark-coloured stool, and temporary staining of the teeth. The solubility of iron sulphate in water is 29.51 g/100 mL (25 °C) and negligible in alcohol [5, 8]. According to the WHO, iron deficiency is the most common nutritional disorder affecting >20% of the global population. Due to the complex physiological as well as dietary factors, only 1 to 2 mg of iron undergoes absorption through the gut enterocyte to the systemic circulation [9, 10]. The bioavailability of the iron sulphate is a major concern. The Biofield Energy Treatment (the Trivedi Effect®) could be an economical approach for the reduction of particle size/crystallite size and improvement of the surface area; that would be helpful for the enhancement of the bioavailability of pharmaceutical/nutraceutical compounds [11, 12].

The human body can release electromagnetic waves in the form of bio-photons that surrounds the body. This electromagnetic energy is generated by the continuous movement of the electrically charged components (ions, cells, etc.) present inside the body. This is collectively known as “Biofield Energy”. Biofield Energy Healer has the capability to harness the energy from the “Universal Energy Field” and can transmit into any living or non-living object(s). The process by which the objects receive the Biofield Energy Treatment from the Biofield Energy Healer(s) and respond into a useful way is called as Biofield Energy Healing Treatment [13-15]. Biofield based Energy Therapies are adopted worldwide to promote health and healing. The National Center of Complementary and Integrative Health (NCCIH) has recognized and accepted Biofield based Energy Healing therapies as a Complementary and Alternative Medicine (CAM) health care approach in addition to other medicines, therapies, and practices such as special diets, deep breathing, yoga, Tai Chi, chiropractic/osteopathic manipulation, Qi Gong, meditation, homeopathy, essential oils, massage, progressive relaxation, guided imagery, acupressure, acupuncture, healing touch,

hypnotherapy, movement therapy, rolfing structural integration, pilates, mindfulness, naturopathy, Ayurvedic medicine, traditional Chinese herbs and medicines, cranial sacral therapy, aromatherapy, Reiki, and applied prayer [16]. The Trivedi Effect®-Consciousness Energy Healing Treatment had been expansively reported with significant results in different scientific fields like agricultural science [17-19], materials science [20-23], cancer research [24, 25], microbiology [26-29], genetics [30, 31], pharmaceutical science [11, 12, 32-35], *etc*.

The physicochemical properties of a medicament play an important role in bioavailability, as these factors have a direct influence on solubility, absorption, and stability of the drug [36]. The specific surface area, particle size, crystalline nature, chemical and thermal behaviour of an atom/ion might be altered by the Energy of Consciousness Healing Treatment (the Trivedi Effect®) through the possible mediation of neutrinos [37]. Thus, in this study the impact of the Trivedi Effect®-Consciousness Energy Healing Treatment on the physicochemical, thermal, and behavioural properties of iron sulphate was evaluated using modern analytical techniques.

2. MATERIALS AND METHODS

2.1. Chemicals and Reagents.

The test sample iron sulphate was purchased from Sigma-Aldrich, India. Similarly, other chemicals used in the experiments also purchased in India.

2.2. Consciousness Energy Healing Treatment Strategies.

The test sample iron sulphate was divided into two parts. One part of iron sulphate was considered as control (no Biofield Energy Treatment was provided), while the second part of iron sulphate was received the Trivedi Effect®-Consciousness Energy Healing Treatment remotely under standard laboratory conditions (for 3 minutes) called the Biofield Energy Treated iron sulphate. This Biofield Energy Treatment was delivered through the healer's unique energy transmission process by a famous Biofield Energy Healer, Mr. Mahendra Kumar Trivedi (USA) to the test item. The control iron sulphate was treated with a "sham" healer who did not have any information about the Biofield Energy Treatment. After that, both the samples were kept in sealed conditions and characterized using modern analytical techniques.

2.3. Characterization.

The powder X-ray diffraction (PXRD) analysis of iron sulphate was performed with the help of PANalytical X'Pert3 Pro [34, 35, 38]. The average crystallites size was calculated using the Scherrer's formula (1)

$$G = k\lambda/\beta\cos\theta \qquad (1)$$

Where G is the crystallite size in nm, λ is the radiation wavelength, k is the equipment constant, β is the full-width half maximum, and θ is the Bragg angle [38, 39].

The particle size distribution (PSD) analysis of iron sulphate powder sample was performed with the help of Malvern Mastersizer 3000, UK instrument using the wet method. Fourier transform infrared (FT-IR) spectroscopy of iron sulphate was performed using Spectrum ES (Perkin Elmer, USA) Fourier transform infrared spectrometer. Ultra violet-visible spectroscopy (UV-Vis) analysis was carried out using Shimadzu UV-2400PC series, Japan. Similarly, the differential scanning calorimetry (DSC) analysis of iron sulphate was performed with the help of DSC Q200, TA instruments. The thermal gravimetric analysis (TGA) thermograms of iron sulphate were obtained with the help of TGA Q50 TA instruments [34, 35, 38].

The % change in crystallite size, peak intensity, particle size, surface area, melting point, latent heat, weight loss and the maximum thermal degradation temperature of the Biofield Energy Treated iron sulphate was calculated compared to the control sample using the following equation 2:

$$\%\ \text{change} = \frac{[\text{Treated} - \text{Control}]}{\text{Control}} \times 100 \qquad (2)$$

3. RESULTS

3.1. Powder X-ray Diffraction (PXRD) Analysis.

PXRD data of both the iron sulphate samples are presented in Table 1. The sharp and intense peaks in PXRD diffractograms of the control and Biofield Energy Treated iron sulphate (Figure 1) indicating that both the samples are crystalline in nature.

The PXRD diffractograms of both the samples showed highest peak intensity (100%) at Bragg's angle (2θ) equal to 18.3° and 18.2°, respectively (Table 1, entry 6 & 7). The Bragg's angle (2θ) of the 28 diffraction peaks in both the samples remained almost same, but the relative intensities of the peaks of the Biofield Energy Treated sample were found to be altered compared to the control sample. The relative intensities of the in the Biofield Energy Treated sample were significantly altered from -87.25% to 338.67% compared to the control sample. The overall crystallite sizes of the in the Biofield Energy Treated sample were significantly altered from -58.33% to 99.84% compared to the control sample. The average crystallite size of the treated iron sulphate was reduced by 5.68% as compared to the control sample.

The relative intensity of each diffraction face on the crystalline compound changes according to the crystal morphology [40], and alterations in the PXRD pattern provide the proof of polymorphic transitions [41, 42]. It has been reported that the Biofield Energy Treatment has the significant ability to produce a new crystalline polymorph by changing the crystal morphology of the pharmaceuticals and nutraceuticals [34, 35, 38]. The significant variations in the crystallite size and relative intensities indicated the modification of the crystal morphology of the Biofield Energy Treated iron sulphate sample compared with the control sample. The Trivedi Effect®-Consciousness Energy Healing Treatment probably led to produce a polymorphic form through the energy transferred into iron sulphate. Polymorphic forms of

pharmaceutical compounds have the significant effects on the drug performance, such as bioavailability, therapeutic efficacy, and toxicity, because their thermodynamic and physicochemical properties are different (probably an improvement) from the original form [43, 44]. Thus, it can be anticipated that Mr. Trivedi's Biofield Energy Treatment could be a very useful method for the production of novel crystal polymorph of iron sulphate that would offer an improvement in its therapeutic performance.

3.2. Particle Size Distribution (PSD) Analysis.

The particle size of both the control and Biofield Energy Treated iron sulphate were investigated and presented in Table 2. It was observed that the particle sizes in the treated iron sulphate at d_{10}, d_{50}, d_{90}, and D(4,3) value was a decreased by 1.54%, 1.12%, 2.51%, and 1.90%, respectively compared to the control sample (Table 2). The surface area of the control and Biofield Energy Treated sample were 24.94 and 26.11 m^2/kg, respectively. The results showed that the surface area of the treated sample was increased by 4.69% compared with the control sample.

The particle size and surface area of any pharmaceutical compounds play a vital role in the solubility, dissolution, absorption, and bioavailability [45-47]. Reduction in the particle size increases the surface area, which enhances the solubility properties of the solid particles as well as the dissolution rate and bioavailability [47, 48]. Thus, it is anticipated that the Trivedi Effect® - Energy of Consciousness Healing Treated iron sulphate could offer better bioavailability than the untreated sample.

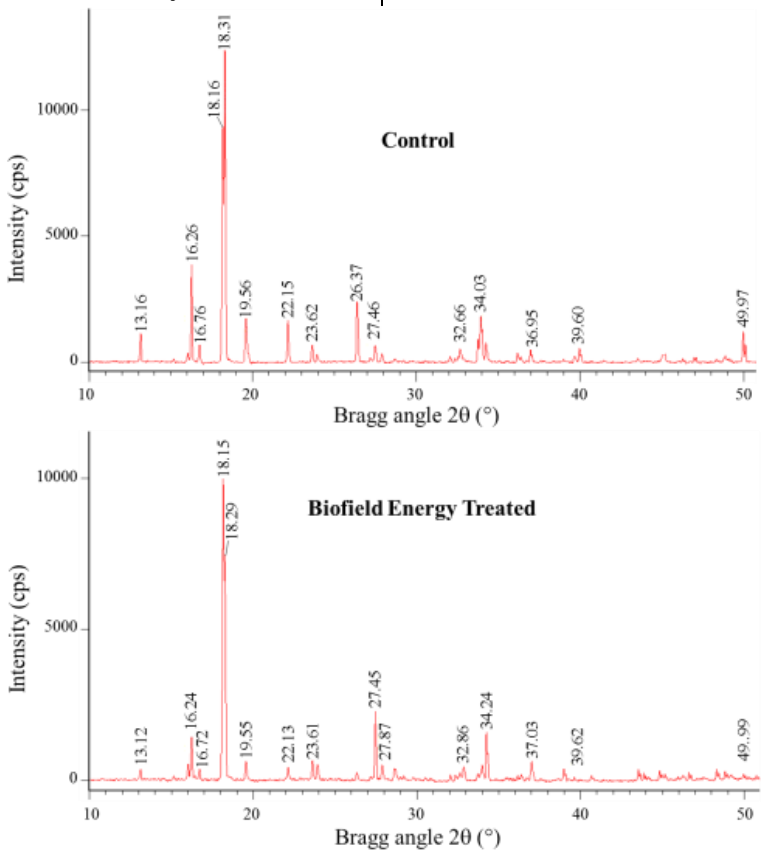

Figure 1. PXRD diffractograms of the control and treated iron sulphate.

Table 1. PXRD data for the control and treated iron sulphate.

Entry No.	Bragg angle (°2θ)	Relative Intensity (%)			Crystallite Size(G, nm)		
		Control	Treated	% Change*	Control	Treated	% Change*
1	13.2	9.21	3.63	-60.59	49.62	49.62	0.00
2	16.1	2.99	5.48	83.28	58.01	49.78	-14.19
3	16.3	31.25	14.60	-53.28	43.56	43.57	0.00
4	16.8	5.57	3.78	-32.14	43.59	58.06	33.20
5	18.2	74.56	100.00	34.12	58.17	58.17	0.00
6	18.3	100. 00	71.95	-28.05	49.93	58.18	16.53
7	19.6	12.98	6.38	-50.85	35.00	38.89	11.12
8	22.2	13.27	4.34	-67.29	35.15	39.06	11.12
9	23.6	5.29	6.33	19.66	35.24	35.24	0.00
10	23.9	2.46	5.28	114.63	50.39	35.26	-30.02
11	26.4	18.75	2.39	-87.25	39.37	50.62	28.59
12	27.5	5.12	22.46	338.67	50.74	59.14	16.54
13	27.9	2.63	5.13	95.06	50.79	50.79	0.00
14	32.1	1.75	1.51	-13.71	71.72	71.72	0.00
15	32.4	1.31	1.66	26.72	71.78	59.81	-16.67
16	32.9	4.30	4.52	5.12	89.79	51.39	-42.76
17	34.3	10.12	15.71	55.24	98.58	59.18	-39.96

Entry No.	Bragg angle (°2θ)	Relative Intensity (%)			Crystallite Size(G, nm)		
		Control	Treated	% Change*	Control	Treated	% Change*
18	34.4	6.17	8.25	33.71	59.18	74.00	25.04
19	36.2	2.84	1.67	-41.20	49.58	59.50	20.00
20	36.4	1.87	1.88	0.53	74.42	37.21	-50.00
21	37.0	3.94	6.50	64.97	59.64	59.65	0.02
22	39.6	1.26	1.13	-10.32	50.10	50.10	0.01
23	43.5	1.14	3.73	227.19	50.75	60.90	20.01
24	45.1	3.76	3.14	-16.49	30.62	61.19	99.84
25	46.3	1.32	1.21	-8.33	51.25	25.63	-49.99
26	46.9	1.58	1.78	12.66	51.38	61.62	19.92
27	48.9	2.13	3.05	43.19	51.77	51.77	-0.02
28	50.0	10.04	1.38	-86.25	62.40	26.00	-58.33

*denotes the percentage change in the relative intensities/crystallite size of the treated sample compared to the control sample.

Table 2. Particle size values (d_{10}, d_{50}, and d_{90}) and surface area of the control and treated iron sulphate.

Parameter	d_{10} (µm)	d_{50} (µm)	d_{90} (µm)	D(4,3) (µm)	Surface area (m^2/Kg)
Control	133	357	798	420	24.94
Biofield Treated	131	353	778	412	26.11
Percent change* (%)	-1.50	-1.12	-2.51	-1.90	4.69

*denotes the percentage change in the particle size and surface area of the treated sample compared to the control sample.

3.3. Fourier Transform Infrared (FT-IR) Spectroscopy.

The FT-IR spectra of control and Biofield Energy Treated samples of iron sulphate are shown in Figure 2. The FT-IR spectra of the control and Biofield Energy Treated iron sulphate showed the clear stretching and bending peaks in the functional group and fingerprint region (Table 3). The broad peaks in the functional group region of the control and Biofield Energy Treated spectra were observed near 3377 cm^{-1}, which might be due to the water molecules in the sample. The spectra showed S=O stretching near 1097 cm^{-1}, and Fe-O stretching near 618 cm^{-1} for both control and Biofield Energy Treated samples. The FT-IR spectra did not display any changes in the vibrational frequencies. Overall results suggested that there was no significant alteration in the structural properties of the Biofield Energy Treated iron sulphate compared to the control sample.

Table 3. FT-IR data of the control and treated iron sulphate.

Mode of vibration	Characteristic absorptions (cm^{-1})		Status
	Control	Biofield Energy Treated	
O-H stretching	3377	3380	very strong, very broad
O-H Bending	1648	1648	medium
S=O stretching	1097	1096	very strong, broad
Fe-O Stretching	618	618	strong, very broad

3.4. Ultraviolet-visible Spectroscopy (UV-Vis) Analysis.

The UV-visible spectra of the control and Biofield Energy Treated iron sulphate are shown in Figure 3. The UV spectrum of control and Biofield Energy Treated sample showed the maximum absorbance at 190 nm (λ_{max}). The peak at 190 nm was showed a minor shift of absorbance maxima from 0.6832 in control to 0.6960 in Biofield Energy Treated sample. There were similar absorbance maxima in the Biofield Energy Treated iron sulphate compared to the control sample.

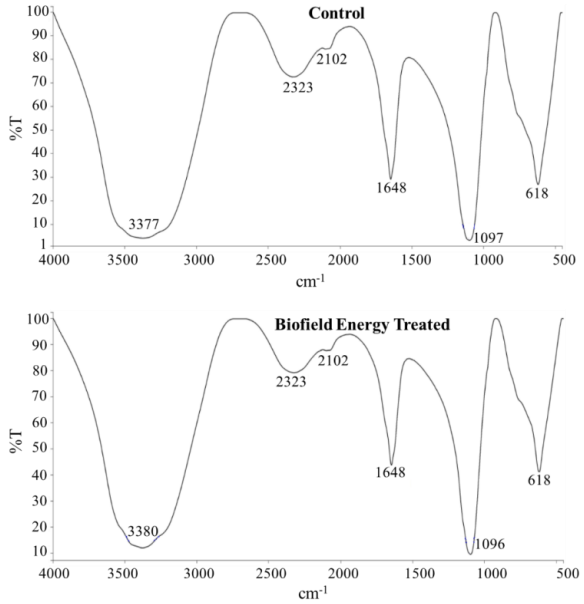

Figure 2. FT-IR spectra of the control and treated iron sulphate.

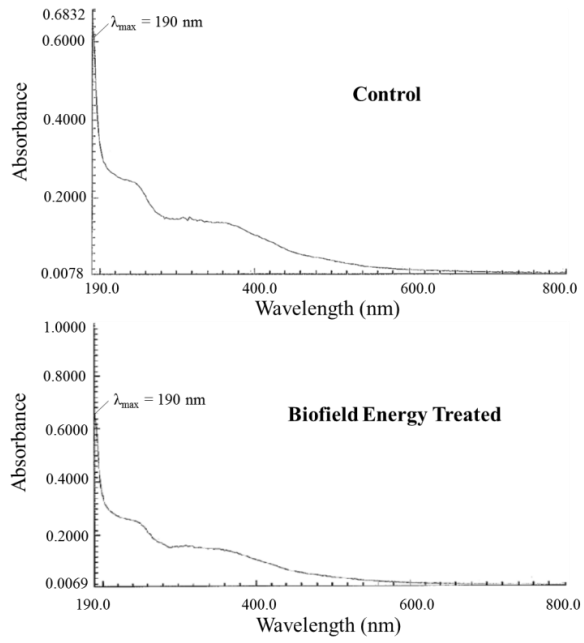

Figure 3. UV-Vis spectra of the control and treated iron sulphate.

3.5. Differential Scanning Calorimetry (DSC) Analysis.

The DSC thermograms of the control and Biofield Energy Treated samples of iron sulphate are presented in Figure 4. The thermograms of the control and treated iron sulphate samples exhibited the presence of the four broad endothermic inflection, which might be due to the melting temperature and dehydration of water molecules of the sample. Scientific literature reported the dehydration behavior of iron sulphate heptahydrate ($FeSO_4•7H_2O$) by using DSC and TGA techniques [49, 50]. Wang *et al.* mentioned 3 peaks in the DSC curve at a heating rate of 10 °C under nitrogen atmosphere. The 1st peak at the temperature below 100 °C, 2nd peak at 85 to 149 °C, and 3rd peak at 247 to 342 °C was due to the dehydration of 7 water molecules from $FeSO_4•7H_2O$ to $FeSO_4•4H_2O$, $FeSO_4•4H_2O$ to $FeSO_4•H_2O$, and $FeSO_4•H_2O$ to $FeSO_4$, respectively. They also concluded that accurate thermal data from the TGA/DSC dehydration experiments depends on various factors like proper selection of the heating rate, particle size, open or closed pan, *etc.* [49].

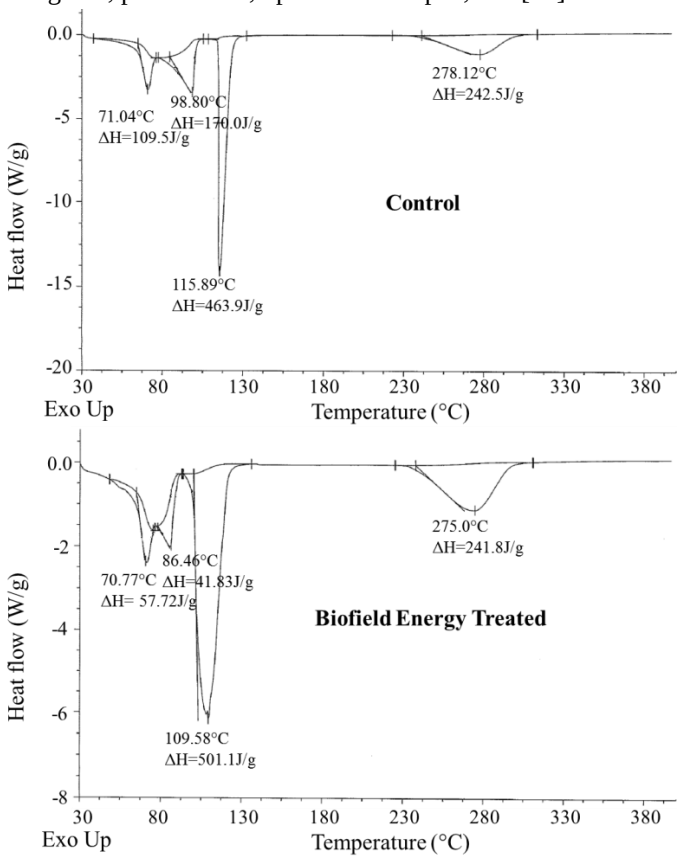

Figure 4. DSC thermograms of the control and treated iron sulphate.

The DSC thermogram of the control iron sulphate heptahydrate exhibited four broad endothermic peaks. The 1st sharp endothermic peak at 71.04 °C was the melting point of the control sample of iron sulphate heptahydrate. Similarly, the 2nd broad endothermic peak at 98.80 °C might be due to the dehydration of 2 molecules of water from $FeSO_4•6H_2O$ to $FeSO_4•4H_2O$. The 3rd sharp endothermic peak at 115.89 ºC, which was due to the removal of 3 molecules of water from $FeSO_4•4H_2O$ to $FeSO_4•H_2O$ and finally a broad endothermic peak at 278.12 °C was found in the control sample due to the dehydration from iron sulphate monohydrate to anhydrous $FeSO_4$. Similarly, the thermograms of the Biofield Energy Treated iron sulphate heptahydrate exhibited the presence of four broad endothermic inflection at 70.8, 86.5, 109.6, 275.0 ºC (Figure 4). The melting temperature of 1st, 2nd, 3rd, and 4th peaks in the Biofield Energy Treated iron sulphate was decreased by 0.28%, 12.45%, 5.44%, and 0.51%, respectively compared to the control sample (Table 4). The latent heat of fusion (ΔH) of 1st, 2nd, and 4th peaks in the Biofield Energy Treated iron sulphate were decreased by 47.29%, 75.39%, and 0.29%, respectively, whereas ΔH of the 3rd peak was increased by 8.02% compared with the control sample. The results suggested that the thermal stability of the Biofield Energy Treated sample was decreased compared with the control sample (Table 4). The data indicated that the treated iron sulphate needed less energy in the form of ΔH to undergo the whole process of melting after Biofield Energy Treatment.

3.6. Thermogravimetric analysis (TGA)/ Differential Thermogravimetric Analysis (DTG).

The TGA thermogram of iron sulphate heptahydrate exhibit four steps of thermal degradation as per the reported literature [49, 50]. The first weight loss occurs between 70 and 90 °C due to the loss of 3 water molecules from $FeSO_4•7H_2O$. The second dehydration step with the loss of 3 water molecules from $FeSO_4•4H_2O$ is responsible for the mass loss between 140 and 200 °C. Consequently, the third weight loss is found between 270 and 350 °C due to the dehydration of $FeSO_4•H_2O$. Final major weight loss between 400 and 830 °C occurs due to the oxidation and dehydration of the other part of monohydrate, sulphate decomposition. The major weight loss occurred in the first (38.30%) and fourth (28.30%) reactions as per the literature [49, 50].

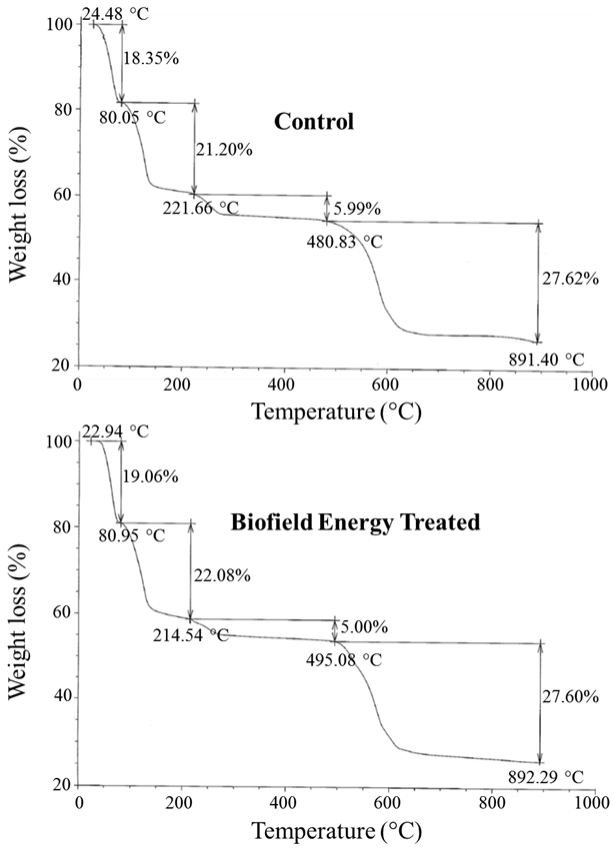

Figure 5. TGA thermograms of the control and treated iron sulphate.

The TGA thermograms of the control and Biofield Energy Treated samples exhibited four steps of thermal degradation (Figure 5), which matched with the reported literature [49, 50]. The percentage weight loss in the Biofield Energy Treated iron sulphate was significantly increased by 3.87% and 4.15% in the 1st

and 2nd steps of degradation, respectively compared with the control sample. The percentage of weight loss in the 3rd and 4th steps of degradation was reduced by 16.67% and 0.07%, respectively, compared with the control sample (Table 5). The overall weight loss in the Biofield Energy Treated iron sulphate was increased by 0.78% compared with the control sample.

The DTG thermograms of the control sample disclosed four peaks (P_1, P_2, P_3, and P_4) with maximum temperature (T_{max}) of 61.62, 127.06, 252.94, and 582.93 °C, respectively (Figure 6). Similarly, the DTG thermograms of the Biofield Energy Treated sample disclosed four peaks P_1, P_2, P_3, and P_4 with maximum temperature (T_{max}) at 62.87, 125.12, 220.97, and 575.54 °C, respectively (Figure 6). The analysis indicated that the T_{max} of the Biofield Energy Treated iron sulphate was slightly increased by 2.03% in the first peak, but the T_{max} of P_2, P_3, and P_4 peaks were decreased by 1.53%, 12.64%, and 1.27%, respectively compared to the control sample (Table 6). As per the literature, with reduction of the particle size decreases the melting point and latent heat of fusion [51]. Overall, TGA/DTG revealed that the thermal stability of the Biofield Energy Treated iron sulphate was decreased as compared to the control sample. Reduced thermodynamic stability favours the enhancement of the dissolution rate and bioavailability of the pharmaceutical solid compound [52].

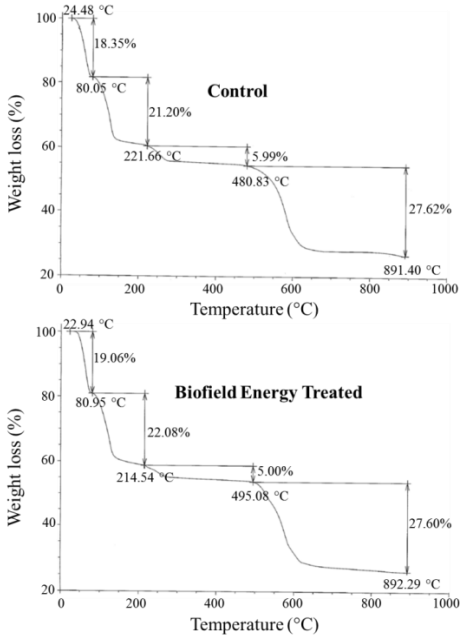

Figure 5. TGA thermograms of the control and treated iron sulphate.

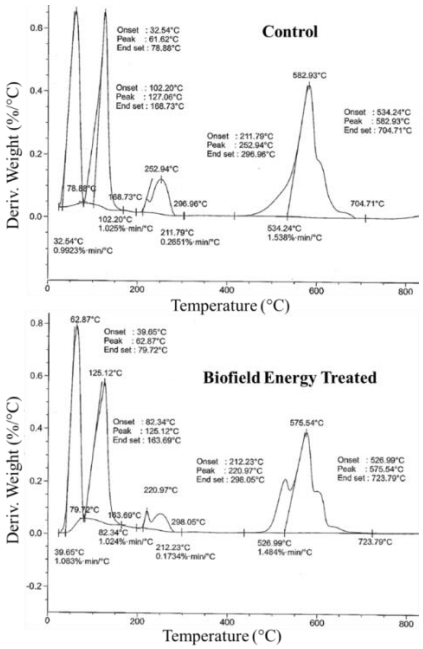

Figure 6. DTG thermograms of the control and treated iron sulphate.

Table 4. The Latent heat of fusion (J/g) and melting point (°C) values for both control and treated samples of iron sulphate.

Sample	Temperature(°C)				ΔH (J/g)			
	1st Peak	2nd Peak	3rd Peak	4th Peak	1st Peak	2nd Peak	3rd Peak	4th Peak
Control Sample	71.0	98.8	115.9	278.12	109.5	170.0	463.9	242.5
Biofield Energy Treated	70.8	86.5	109.6	275.0	57.72	41.83	501.1	241.8
% Change*	-0.28	-12.45	-5.44	-0.51	-47.29	-75.39	8.02	-0.29

ΔH: Latent heat, *denotes the percentage change of the treated sample compared to the control sample.

Table 5. Thermal degradation steps of the control and treated samples of iron sulphate.

Step	Temperature(°C)		%Weight Loss		% Change*
	Control	Treated	Control	Treated	
1st step of degradation	80.05	80.95	18.35	19.06	3.87
2nd step of degradation	221.66	214.54	21.20	22.08	4.15
3rd step of degradation	480.83	495.08	6.00	5.00	-16.67
4th step of degradation	891.40	892.29	27.62	27.60	-0.07
Total weight loss			73.17	73.74	0.78

*denotes the percentage change of the treated sample compared to the control sample.

Table 6. Derivative thermal degradation steps of the control and treated samples of iron sulphate.

Description	P_1 (°C)	P_2 (°C)	P_3 (°C)	P_4 (°C)
Control Sample	61.62	127.06	252.94	582.93
Biofield Energy Treated	62.87	125.12	220.97	575.54
% Change*	2.03	-1.53	-12.64	-1.27

P_1, P_2, P_3, and P_4: peak 1, 2, 3, and 4. *denotes the percentage change of the treated sample with respect to the control sample.

4. CONCLUSIONS

The experimental results revealed that the Trivedi Effect® - Consciousness Energy Healing Treatment has a significant impact on the physicochemical, thermal, and behavioural properties of iron sulphate. The powder XRD relative peak intensities and

crystallite size of the treated iron sulphate were significantly altered ranging from -87.25% to 338.67% and from -58.33% to 99.84%, respectively compared with the control sample. The average crystallite size of the treated sample was significantly decreased by 5.68% compared with the control sample. The particle size values of the treated sample was decreased by 1.54% (d_{10}), 1.12% (d_{50}), 2.51% (d_{90}), and 1.90% {D(4,3)} and the surface area was increased by 4.69% compared with the control sample. The melting temperature of the four peaks (1^{st} -4^{th}) of the treated sample was decreased by 0.28%, 12.45%, 5.44%, and 0.51%, respectively compared to the control sample. The ΔH_{fusion} of 1^{st}, 2^{nd}, and 4^{th} peaks in the treated sample was decreased by 47.29%, 75.39%, and 0.29%, respectively, whereas 3^{rd} peak was increased by 8.02% compared with the control sample. The thermograms of both the samples exhibited four steps of thermal degradation and the weight loss in the treated sample were increased by 0.78% compared with the control sample. The maximum thermal melting temperature of the treated iron sulphate was slightly increased by 2.03% in the 1^{st} peak but decreased by 1.53%, 12.64%, and 1.27% in the 2^{nd}, 3^{rd}, and 4^{th} peaks, respectively compared to the control sample. Overall, the thermal analysis indicated that the thermal stability of the Biofield Energy Treated iron sulphate was altered compared to the control sample. Thus, the Energy of Consciousness Healing Treatment (the Trivedi Effect®) might lead to produce a new polymorphic form of iron sulphate which would be more soluble, and bioavailable compared with the untreated sample. The Biofield Energy Treated iron sulphate would be very useful to design more efficacious nutraceutical and pharmaceutical formulations which might offer better therapeutic response against iron deficiency anemia and other industrial application in the chemical industry.

5. REFERENCES

1. Reddy, S.N.; Rao, P.S.; Ravikumar, R.V.; Reddy, B.J.; Reddy, Y.P. Spectral investigations on melanterite mineral from France. *Spectrochim Acta A Mol Biomol Spectrosc* **2001**, *57*: 1283, https://doi.org/10.1016/S1386-1425(00)00475-3.
2. Lide, D.R. Ed. *CRC Handbook of Chemistry and Physics (90th ed.)*. Boca Raton, Florida: CRC Press, 2009.
3. Jančovičová, V.; Čeppan, M.; Havlínová, B.; Reháková, M.; Jakubíková, Z. Interactions in iron gall inks. *Chemical Papers* **2007**, *61*, 391-397, https://doi.org/10.2478/s11696-007-0053-0.
4. Koenig, R.; Kuhns, M. *Control of iron chlorosis in ornamental and crop plants*. Utah State University, Salt Lake City, 2010.
5. Santiago, P. Ferrous versus ferric oral iron formulations for the treatment of iron deficiency: A clinical overview. *Scientific World Journal* **2012**, *2012*, https://doi.org/10.1100/2012/846824.
6. Fenton, H.J.H. Oxidation of tartaric acid in presence of iron. *J Chem Soc* **1894**, *65*, 899-911, https://doi.org/10.1039/CT8946500899.
7. Hayyan, M.; Hashim, M.A.; Al Nashef, I.M. Superoxide ion: Generation and chemical implications. *Chem Rev* **2016**, *116*, 3029-3085, https://doi.org/10.1021/acs.chemrev.5b00407.
8. Bothara, K.G. *Inorganic Pharmaceutical Chemistry*. 9th Edition, Nirali Prakashan, Pune, India, 2007.
9. Zariwala, M.G.; Somavarapu, S.; Farnaud, S.; Renshaw, D. Comparison study of oral iron preparations using a human intestinal model. *Sci Pharm* **2013**, *81*, 1123-1139, https://doi.org/10.3797/scipharm.1304-03
10. Zimmermann, M.B.; Hurrell, R.F. Nutritional iron deficiency. *Lancet* **2007**, *370*: 511-520, https://doi.org/10.1016/S0140-6736(07)61235-5.
11. Branton, A.; Trivedi, M.K.; Trivedi, D.; Nayak, G. Evaluation of the physicochemical and thermal properties of the biofield energy healing treated ofloxacin. *J Pharm Pharmaceutics* **2018**, 5: 80-87, https://doi.org/10.15436/2377-1313.18.1965.
12. Trivedi D, Trivedi MK, Branton A, Nayak G, Jana S Consciousness energy healing treatment: Impact on the physicochemical and thermal properties of ascorbic acid. *Food Nutr Current Res* **2019**, 2, 164-173.
13. Rubik, B. The biofield hypothesis: Its biophysical basis and role in medicine. *J Altern Complement Med* **2002**, *8*, 703-717, https://doi.org/10.1089/10755530260511711.
14. Nemeth, L. Energy and biofield therapies in practice. *Beginnings* **2008**, *28*, 4-5.
15. Rivera-Ruiz, M.; Cajavilca, C.; Varon, J. Einthoven's string galvanometer: The first electrocardiograph. *Tex Heart Inst J* **2008**, *35*, 174-178.
16. Koithan, M. Introducing complementary and alternative therapies. *J Nurse Pract* **2009**, *5*, 18-20, https://dx.doi.org/10.1016%2Fj.nurpra.2008.10.012.
17. Trivedi, M.K.; Branton, A.; Trivedi, D.; Nayak, G.; Mondal S.C. Morphological characterization, quality, yield and DNA fingerprinting of biofield energy treated alphonso mango (*Mangifera indica* L.). *Journal of Food and Nutrition Sciences* **2015**, *3*, 245-250, http://dx.doi.org/10.5281/zenodo.192448.
18. Trivedi, M.K.; Branton, A.; Trivedi, D.; Nayak, G.; Mondal, S.C.; Jana, S. Evaluation of plant growth, yield and yield attributes of biofield energy treated mustard (*Brassica juncea*) and chick pea (*Cicer arietinum*) seeds. *Agriculture, Forestry and Fisheries* **2015**, *4*, 291-295, http://dx.doi.org/10.5281/zenodo.192893.
19. Trivedi, M.K.; Branton, A.; Trivedi, D.; Nayak, G.; Mondal, S.C.; Jana, S. Evaluation of plant growth regulator, immunity and DNA fingerprinting of biofield energy treated mustard seeds (*Brassica juncea*). *Agriculture, Forestry and Fisheries* **2015**, *4*, 269-274, http://dx.doi.org/10.5281/zenodo.181865.
20. Trivedi, D.; Trivedi, M.K.; Branton, A.; Nayak, G.; Jana, S. Consciousness Energy Healing Treatment: Impact on Physicochemical and Thermal Properties of Zinc. Modern Approaches on Material Science. *Mod App Matrl Sci* **2019**, 1, 95-101, https://doi.org/ 10.32474/MAMS.2019.01.000116.
21. Dahryn, T.; Mahendra, K.T.; Alice, B.; Gopal, N.; Snehasis, J. Evaluation of the physicochemical and thermal properties of antimony: Influence of the energy of consciousness healing treatment. *Op Acc J Bio Eng & Bio Sci* **2019**, 3, 303-309. http://dx.doi.org/10.32474/OAJBEB.2019.03.000163.
22. Nayak, G.; Trivedi, M.K.; Branton, A; Trivedi, D.; Jana, S. Physicochemical and thermal properties of consciousness energy healing treated hydroxypropyl β-cyclodextrin. *Med & Analy Chem Int* J **2018**, 2: 000124. http://dx.doi.org/ 10.23880/macij-16000124 .
23. Trivedi, M.K.; Nayak, G.; Patil, S.; Tallapragada, R.M.; Latiyal, O. Characterization of physical and structural properties of brass powder after biofield treatment. *J Powder Metall Min* **2015**, *4*, 134.
24. Trivedi, M.K.; Patil, S.; Shettigar, H.; Mondal, S.C.; Jana, S. The potential impact of biofield treatment on human brain tumor

cells: A time-lapse video microscopy. *J Integr Oncol* **2015**, *4*, 141, https://doi.org/10.4172/2329-6771.1000141.

25. Trivedi, M.K.; Patil, S.; Shettigar, H.; Gangwar, M.; Jana. S. *In vitro* evaluation of biofield treatment on cancer biomarkers involved in endometrial and prostate cancer cell lines. *J Cancer Sci Ther* **2015**, *7*, 253-257, https://doi.org/10.4172/1948-5956.1000358.

26. Trivedi, M.K.; Patil, S.; Shettigar, H.; Mondal, S.C.; Jana, S. *In vitro* evaluation of biofield treatment on *Enterobacter cloacae*: Impact on antimicrobial susceptibility and biotype. *J Bacteriol Parasitol* **2015**, *6*, 241, https://doi.org/10.4172/2155-9597.1000241.

27. Trivedi, M.K.; Patil, S.; Shettigar, H.; Mondal, S.C.; Jana, S. Evaluation of biofield modality on viral load of Hepatitis B and C Viruses. *J Antivir Antiretrovir* **2015**, *7*, 083-088, https://doi.org/10.4172/jaa.1000123.

28. Trivedi, M.K.; Patil, S.; Shettigar, H.; Mondal, S.C.; Jana, S. An impact of biofield treatment: Antimycobacterial susceptibility potential using BACTEC 460/MGIT-TB System. *Mycobact Dis* **2015**, *5*, 189, https://dx.doi.org/10.4172/2161-1068.1000189.

29. Trivedi, M.K.; Branton, A.; Trivedi, D.; Nayak, G.; Mondal, S.C.; Jena, S. Antimicrobial sensitivity, biochemical characteristics and biotyping of *Staphylococcus saprophyticus*: An impact of biofield energy treatment. *J Women's Health Care* **2015**, *4*, 271, https://doi.org/10.4172/2161-1068.1000189.

30. Trivedi, M.K.; Branton, A.; Trivedi, D.; Nayak, G.; Mondal. S.C.; Jana, S. Evaluation of antibiogram, genotype and phylogenetic analysis of biofield treated *Nocardia otitidis*. *Biol Syst Open Access* **2015**, *4*, 143, https://doi.org/10.4172/2161-1068.1000189.

31. Trivedi, M.K.; Branton, A.; Trivedi, D.; Nayak, G.; Charan, S.; Mondal, S.J. Phenotyping and 16S rDNA analysis after biofield treatment on *Citrobacter braakii*: A urinary pathogen. *J Clin Med Genom* **2015**, *3*, 129, http://dx.doi.org/10.4172/2332-0672.1000129.

32. Nayak, G.; Trivedi, M.K.; Branton, A.; Trivedi, D.; Jana, S. Consciousness energy healing treatment: Impact on physicochemical and thermal properties of silver sulfadiazine. *Journal of advanced pharmaceutical science and technology* **2018**, 2, 1-13, http://dx.doi.org/ 10.14302/issn.2328-0182.japst-18-2517.

33. Nayak, G.; Trivedi, M.K.; Branton, A.; Trivedi, D.; Jana, S. Evaluation of the consciousness energy healing treated berberine chloride using PXRD, PSA, and DSC Analysis. *Food Sci Nutr Technol* **2018**, 3, 000168, https://doi.org/ 10.23880/fsnt-16000168.

34. Trivedi, M.K.; Branton, A.; Trivedi, D.; Nayak, G.; Balmer, A.J.; Anagnos, D.; Kinney, J.P.; Holling, J.M.; Balmer, J.A.; Duprey-Reed, L.A.; Parulkar, V.R.; Panda, P.; Sethi, K.K.; Jana, S. Study of the energy of consciousness healing treatment on physical, structural, thermal, and behavioral properties of zinc chloride. *Modern Chemistry* **2017**, *5*, 19-28, https://doi.org/10.11648/j.mc.20170502.11.

35. Trivedi, M.K.; Branton, A.; Trivedi, D.; Nayak, G.; Balmer, A.J.; Duprey-Reed, L.A.; Parulkar, V.R.; Panda, P.; Sethi, K.K.; Jana, S. Evaluation of physicochemical, spectral, thermal and behavioral properties of the biofield energy healing treated sodium selenate. *Science Journal of Chemistry* **2017**, 5, 12-22, https://doi.org/10.11648/j.sjc.20170502.11.

36. Chereson. R. Bioavailability, bioequivalence, and drug selection. In: *Makoid CM, Vuchetich PJ, Banakar UV (Eds) Basic pharmacokinetics* (1st Edn) Pharmaceutical Press, London, 2009.

37. Trivedi, M.K.; Mohan, T.R.R. Biofield energy signals, energy transmission and neutrinos. *American Journal of Modern Physics* **2016**, *5*, 172-176, https://doi.org/10.11648/j.ajmp.20160506.12.

38. Trivedi, M.K.; Branton, A.; Trivedi, D.; Nayak, G.; Balmer, A.J. Duprey-Reed, L.A.; Parulkar, V.R.; Panda, P.; Sethi, K.K.; Jana, S. Evaluation of physicochemical, thermal, structural, and behavioral properties of magnesium gluconate treated with energy of consciousness (the Trivedi Effect®). *Journal of Drug Design and Medicinal Chemistry* **2017**, *3*, 5-17, https://doi.org/10.11648/j.jddmc.20170301.12.

39. Langford, J.I.; Wilson, A.J.C. Scherrer after sixty years: A survey and some new results in the determination of crystallite size. *J Appl Cryst* **1978**, *11*, 102-113, https://doi.org/10.1107/S0021889878012844

40. Inoue, M.; Hirasawa, I. The relationship between crystal morphology and XRD peak intensity on $CaSO_4.2H_2O$. *J Crystal Growth* **2013**, *380*, 169-175, https://doi.org/10.1016/j.jcrysgro.2013.06.017.

41. Raza, K.; Kumar, P.; Ratan, S.; Malik, R.; Arora, S. Polymorphism: The phenomenon affecting the performance of drugs. *SOJ Pharm Pharm Sci* **2014**, *1*, 10, http://dx.doi.org/10.15226/2374-6866/1/2/00111.

42. Brittain, H.G. *Polymorphism in pharmaceutical solids in Drugs and Pharmaceutical Sciences*, 2nd Edn; Informa Healthcare USA, Inc., New York, Volume 192, 2009.

43. Censi. R.; Martino, P.D. Polymorph impact on the bioavailability and stability of poorly soluble drugs. *Molecules* **2015**, *20*, 18759-18776, https://doi.org/10.3390/molecules201018759

44. Blagden, N.; de Matas, M.; Gavan, P.T.; York, P. Crystal engineering of active pharmaceutical ingredients to improve solubility and dissolution rates. *Adv Drug Deliv Rev* **2007**, *59*: 617-630, https://doi.org/10.1016/j.addr.2007.05.011.

45. Chereson, R. Bioavailability, bioequivalence, and drug selection. In*: Makoid CM, Vuchetich PJ, Banakar UV (Eds) Basic pharmacokinetics* (1st Edn); Pharmaceutical Press, London, 2009.

46. Khadka, P.; Ro, J.; Kim, H.; Kim, I.; Kim, J.T.; Kim, H.; Cho, J.M.; You, G.; Lee, J. Pharmaceutical particle technologies: An approach to improve drug solubility, dissolution and bioavailability. *Asian J Pharm Sci* **2014**, *9*, 304-316, https://doi.org/10.1016/j.ajps.2014.05.005.

47. Mosharrof, M.; Nyström, C. The effect of particle size and shape on the surface specific dissolution rate of microsized practically insoluble drugs. *Int J Pharm* **1995**, *122*, 35-47, https://doi.org/10.1016/0378-5173(95)00033-F.

48. Buckton, G.; Beezer, A.E. The relationship between particle size and solubility. *Int J Pharmaceutics* **1992**, *82*, 7-10, https://doi.org/10.1016/0378-5173(92)90184-4.

49. Wang, T.; Debelak, K.A.; Roth, J.A. Dehydration of iron (II) sulfate heptahydrate. *Thermochimica Acta* **2007**, *462*, 89-93, https://doi.org/10.1016/j.tca.2007.07.001.

50. Földvári, M. Handbook of thermogravimetric system of minerals and its use in geological practice. *Occasional Papers of the Geological Institute of Hungary, Budapest* **2011**, *13*.

51. Zhang, M.; Efremov, M.Y.; Schiettekatte, F.; Olson, E.A.; Kwan, A.T.; Lai, S.L.; Wisleder, T.; Greene, J.E.; Allen, L.H. Size-dependent melting point depression of nanostructures: Nanocalorimetric measurements. *Physical Review B* **2000**, *62*, 10548, https://doi.org/10.1103/PhysRevB.62.10548.

52. Zhao, Z.; Xie, M.; Li, Y.; Chen, A.; Li, G.; Zhang, J.; Hu, H.; Wang, X.; Li, S. Formation of curcumin nanoparticles *via* solution-enhanced dispersion by supercritical CO_2. *Int J Nanomedicine* **2015**, *10*, 3171-3181, https://doi.org/10.2147/IJN.S80434.

6. ACKNOWLEDGEMENTS

The authors are grateful to GVK Biosciences Pvt. Ltd., Trivedi Science, Trivedi Global, Inc., Trivedi Testimonials, and Trivedi Master Wellness for their assistance and support during this work.